

**THEORETICAL APPROACH OF THE INTERACTION
BETWEEN A HUMAN HEAD MODEL AND A MOBILE
HANDSET HELICAL ANTENNA USING NUMERICAL
METHODS**

**N. K. Kouveliotis, S. C. Panagiotou, P. K. Varlamos
and C. N. Capsalis**

Division of Information Transmission Systems
and Material Technology
School of Electrical and Computer Engineering
National Technical University of Athens
9, Iroon Polytechniou Str., 157 73, Zografou, Athens, Greece

Abstract—The interaction of a helical antenna, mounted on a mobile handset, with a human head phantom is investigated in this paper. Using the Genetic Algorithms (GA) technique combined with the Method of Moments (MoM), an optimization of the antenna structure is achieved regarding the input impedance at the operating frequency. The Finite Difference Time Domain (FDTD) method is then applied to simulate the handset's function in the close region of a spherical homogeneous and heterogeneous head phantom. A formula, based on an application of an existing model proposed by Kuster and Balzano for dipole antennas, provides a rather accurate prediction of the induced Specific Absorption Rate (SAR) values in the human head due to the radiating helical antenna. The concept of relating the SAR to the current on the antenna is used in this study to formulate the final expression. Moreover, using the theory of regression, the results of the calculated peak or average SAR are correlated with the distance between the antenna and phantom and with the standing wave ratio (SWR) at the antenna feed point. Thus, the conception that the SAR is indeed related to the antenna operational parameters is reinforced by the outcome of the current study.

1. INTRODUCTION

The recent widespread use of cellular telecommunications has urged the worldwide mobile terminals manufacturers toward the development of handsets with improved appearance and characteristics. The size of the phone's antenna is a key issue in designing more compact mobile transceivers without distorting its radiation and operational properties. For this reason, the use of the helical antenna was introduced, which provides equivalent radiation characteristics compared with monopole antennas, while exhibiting a wider impedance bandwidth and having the advantage of being circularly and linearly polarized. Thus, it can be used both in mobile and satellite communications.

Kraus [1] has been the inventor of this type of antenna in 1946 and has described two radiating modes, the axial and the normal mode. The first one is achieved when the diameter of each loop consisting the helix as well as the spacing between the turns are several fractions of the wavelength λ at the operating frequency (Kraus proposed a circumference length equal to λ of being adequate for the helix to perform a maximum radiation along the axial orientation of the antenna and exhibit circular polarization). The normal mode helical antenna (NMHA) was constructed so as to have a length sufficiently less than the operating wavelength. Then, the maximum radiation is observed at the plane normal to the helix axis and the field appears to be generally elliptically polarized. With an appropriate choice of its dimensions, the helix may radiate with a circular or a linear polarization. Consequently, the normal mode operation is preferred when a handset with a helical antenna is used for mobile communications, approximating the operation of the long standing in the past monopole-like terminals.

The operation of the helical antenna, either mounted on a mobile handset or not, has been the subject of a sufficient number of studies in the recent literature. This investigation has been attained with the application of the most popular numerical methods, like the Finite Difference Time Domain (FDTD) method [2] and the Method of Moments (MoM) [3]. However, whereas the enforcement of the MoM to the helical antenna simulation, by considering the structure of the antenna as a sequence of wire segments, is at most cases direct, the FDTD method application appears to have some drawbacks. The most important of these is the fact that, due to the complex formation of the helix, the FDTD grid size should be sufficiently small to accurately model the antenna under study. This confinement is in most cases non practical, considering the emerging large computational time, and consequently several alternatives have been proposed.

In [4–6] the standard helix antenna mounted on a mobile handset is replaced by an equivalent square-helix structure in order to be accurately modeled within the FDTD scheme. The results obtained appear to be rather approximate, compared with those arising from the application of the MoM or conducted measurements. The concept of considering the helical antenna as a sequence of dipoles and loops (or equivalently as a series of electric and magnetic sources) is introduced in [7,8], where good agreement is observed between the calculated radiation pattern and experimental results. A fine resolution modeling of the helix was obtained in [9], with the application of the graded-mesh FDTD code [10] leading to consistency with the MoM outcome. In [11], the appropriate edge components of the FDTD cells of the helical wire were set to zero, providing a sufficient representation of the antenna radiation compared with the MoM. Furthermore, in [12] a square-helix structure was analyzed with the FDTD method and compared with a proposed hybrid Green/MoM technique.

The performance of the helical handset antenna in the vicinity of a biological tissue has also gained sufficient attention in the recent literature. The presence of the human head significantly distorts the circular polarization pattern of a helix mounted on a mobile handset, as it is mentioned in [6], leading in an increase in the axial ratio. When compared to a monopole antenna, a helix of an about 40% smaller length appears to have a narrower impedance bandwidth as reported in [4] while inducing higher values of Specific Absorption Rate (SAR) at the mobile communications frequencies. A combination of a monopole and a helix antenna [9], provides lower SAR values at 1800 MHz compared to its radiation at 900 MHz, when the realistic GSM standard input power is supplied at the investigated antenna. A study of the electromagnetic field introduced on a human head model by a Terrestrial Trunked Radio (TETRA) mobile system handset equipped with a helical antenna, revealed that the resulting SAR values are under the limits set by the ICNIRP specification [11].

The variation of the SAR level induced in the human body regarding the distance or the basic antenna characteristics (e.g., reflection coefficient, input impedance, current) has been a matter of research in a significant number of studies. In [13], an estimation of the spatial peak SAR is provided depending on the current on the antenna and on the conductivity and permittivity of the human tissue. The proposed approximation formula supplies rather accurate assessment of the spatial peak SAR with respect to different distances between antenna and phantom, with an uncertainty of 3 dB, and can be generalized for spheres with large diameters and heterogeneous bodies. The electromagnetic field induced in a two-layer plane phantom by a

dipole close and parallel to one side of the head, with respect to the distance, is introduced in [14]. The induced field in the phantom is determined by the amplitude and distribution of the dipole's current. The aforementioned studies are both verified in [15] where a half-wavelength dipole antenna is positioned near a uniform semi-infinite plane, a uniform sphere and a uniform or realistic head model.

In this paper, a helical antenna above a conductive box representing the mobile handset is considered. With the application of the method of Genetic Algorithms [16] in conjunction with the MoM, an optimization of the antenna structure is performed concerning the driving point input impedance. Then, the FDTD method is enforced to simulate the operation of the helical handset both in the free space environment and near a homogeneous or heterogeneous sphere representing the human head. The peak and average SAR values are computed together with the antenna input impedance and an approximation formula, based on the concept presented in [13], is applied. This expression provides rather accurate results of the peak SAR values induced in the human head in terms of the current on the antenna. A correlation between the peak and average SAR values and the SWR on the helix, based on the regression theory [17], demonstrates that the absorption mechanism at the user's head can be predicted by means of data from the handset antenna. This latter suggestion was indeed verified for dipole antennas by the findings presented in [18–20].

2. OPTIMIZATION OF THE HANDSET ANTENNA

The structure under study is depicted in Figure 1(a). It consists of a helix antenna placed above a conductive rectangular box. At a first stage, the antenna was simulated with the MoM using the Super Numerical Electromagnetic Code (SNEC) package [21], through the composition of a new SNEC structure. As shown in Figure 1(b), the antenna under investigation is implemented within SNEC as a constitution of wire segments. The segment length was chosen to be 0.0096λ where λ is the wavelength at the frequency of propagation ($f = 900$ MHz). To avoid errors produced by the application of the MoM, the helix and the supporting wire were positioned at a height of 3.2 mm above the conducting box. The genetic algorithms technique module [16] incorporated in the SNEC package was employed to find the optimum handset antenna, considering the resonance at the operating frequency. Each GA solution string of the helix geometry (representing the corresponding varying parameters) comprised possible values of the space between the helix turns, the helix length, the radius of the

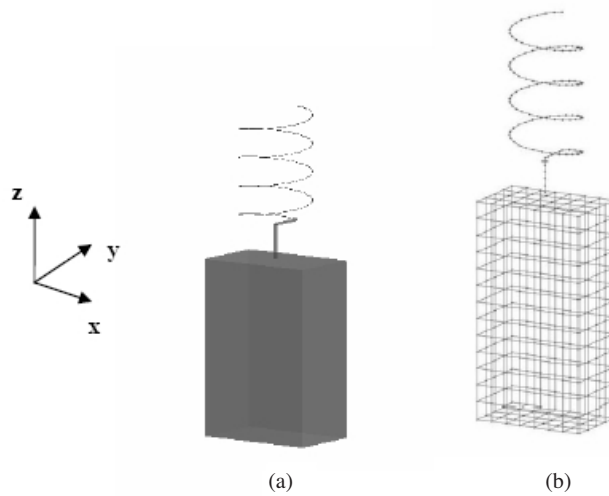


Figure 1. Helical handset structure and its implementation in SNEC.

bottom and top turns, the height of the helix above the conductive box and the dimensions of the handset (height, length and width).

The objective function deployed to obtain desired input impedance level is expressed as

$$of = \left(VSWR_{DES} / VSWR \right)^2 \quad (1)$$

where, $VSWR_{DES}$, $VSWR$ are the desired and computed values of the Voltage Standing Wave Ratio, respectively. The requirement of $VSWR_{DES} = 2$ was set. GAs of 250 generations (60 individuals/generation) were used at 900 MHz. The selection method was population decimation, while adjacent fitness pairing was the mating scheme. The crossover point was chosen randomly and each chromosome was divided at a gene level. The mutation probability was equal to 0.15 [16]. The variation intervals of the GA structure parameters and the final results of the implementation of the GA algorithm are depicted in Table 1.

As long as the optimization procedure is complete, the MoM method was enforced to compute the characteristics of the resultant antenna. The SNEC package was again utilized and gave an input impedance $Z_{in} = 52.72 + 13.37 \Omega$ of the antenna structure at 900 MHz. This value is very close to resonance with a $VSWR = 1.3$ and consequently this particular helical handset with the parameters contained in Table 1 was chosen to be studied in the following with

Table 1. GA structure parameters, variation intervals and simulation results at 900 MHz.

| GA structure parameters | Variation intervals (mm) | Results (mm) |
|-------------------------|--------------------------|--------------|
| Turns spacing | 3.2 – 12.8 | 12.8 |
| Length | 19.2 – 60.8 | 51.2 |
| Base radius | 3.2 – 16 | 12.8 |
| Top radius | 3.2 – 16 | 12.8 |
| Height from ground | 3.2 – 16 | 12.8 |
| Length of Box | 28.8 – 41.6 | 41.6 |
| Width of Box | 9.6 – 28.8 | 25.6 |
| Height of Box | 80 – 121.6 | 80 |

the FDTD method. In the next section, further characteristics of the antenna behavior are computed as a means to compare the results of the application of the MoM and the FDTD method.

3. FDTD IMPLEMENTATION OF THE HELICAL HANDSET

The application of the FDTD scheme to a helix antenna is a rather complicated issue, as it has already been mentioned, due to the small spatial resolution that is demanded to accurately model such a complex structure, in contradiction to the rather straightforward FDTD modeling of other common antennas such as a $\lambda/4$ monopole antenna [22], a microstrip patch antenna [23] or a square slot antenna [24]. In this study, in order to model the helix through the FDTD, the coordinates of each segment comprising the MoM implementation of the helical handset were used. At each selected segment, the appropriate edge electric field components were set to zero following the procedure proposed in [11]. A sinusoidal voltage was applied at the gap of 3.2 mm, which separates the helix from the conductive box. The form of the applied voltage was:

$$V_s(t) = \sin(2\pi ft) \quad (2)$$

where $f = 900$ MHz is the operating frequency.

According to FDTD principles [2], the spatial size of the applied grid was selected to be 1.7 mm, so as to have a convergence in the numerical results. For this reason, a total simulation time of 2000 steps

was chosen as well. A Generalized Perfectly Matched Layer (GPML) [25] of 8 layers was enforced at the boundaries of the applied grid, which were chosen to be 20 cells away from the simulated antenna.

The application of the FDTD method to this particular helical handset returned a value for the antenna input impedance equal to $Z_{in} = 54.33 + j1.42 \Omega$ with a $VSWR = 1.091$ and is apparently very close to resonance. A comparison between the values of Z_{in} computed through the MoM and the FDTD method yields a rather satisfying result considering the difficulty in modeling the helix through the latter method. The far field patterns of the simulated antenna are computed with the aid of the MoM (using the SNEC package) and the FDTD method (using the procedure described analytically in [2]) and the results are depicted in Figure 2 for each representative plane xy , yz and zx .

The plotted patterns reveal that the far field radiation of the helix antenna appears to have a similar behavior, for each of the two arithmetic techniques simulating the problem under study. An almost omni directional radiation is observed at the $\theta = 90^\circ$ plane, which is justified by the handset's symmetrical structure. A maximum radiation at the $(\varphi = 0^\circ, \theta = 90^\circ)$, $(\varphi = 0^\circ, \theta = 270^\circ)$, $(\varphi = 90^\circ, \theta = 90^\circ)$ and $(\varphi = 90^\circ, \theta = 270^\circ)$ directions is noticed in Figure 2, and this is prospective due to the normal mode helical operation deriving from the dimensions cited in Table 1. Although the absolute gain values at each direction for each arithmetic technique show to differ, the fact that the shape of the far field radiation is identical provides a sufficient verification of the FDTD code applied, compared to MoM results generated through the SNEC program. Moreover, the goal of the study at this stage is not the optimization of the antenna radiation properties, but to provide a resonant handset, thus, with no losses generated by improper match, which will be consecutively utilized for an assessment of the energy absorption by a human head model.

4. SAR COMPUTATION

4.1. Homogeneous Phantom

A homogeneous sphere filled with human tissue simulating liquid was added in the vicinity of the helical handset (see Figure 3) and the SAR induced in the human model was calculated.

The sphere had a diameter of $D_S = 20.4$ cm and the tissue that it contained had a relative permittivity of $\epsilon_r = 45.81$, a conductivity of $\sigma = 0.77$ S/m and a density of $\rho = 1030$ Kg/m³. These dielectric parameters were chosen according to [26] for the frequency of 900 MHz

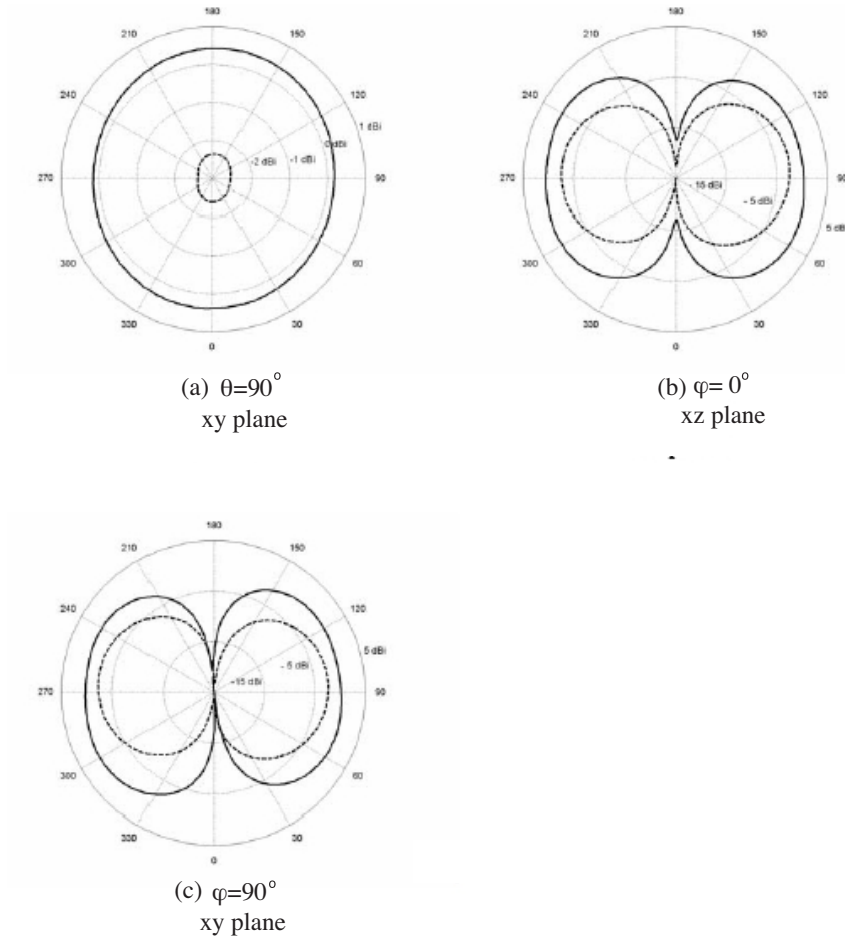


Figure 2. Radiation patterns in the (a) xy , (b) xz and (c) zy planes. The solid lines represent the results from the MoM calculations and the dashed the results from the FDTD method.

and for brain simulating tissue. The same parameters of the free space FDTD implementation were also used in this configuration and the peak values of the spatial SAR were computed as well as the peak average values of SAR over 1 g and 10 g of tissue. The results with respect to the distance d between antenna (axis of helix) and outer surface of the human phantom are summarized in Figure 4. Hereafter, the presented values of SAR have been normalized to the antenna actual radiated power at each examined location.

As it is drawn out from this latter figure, an exponential variation

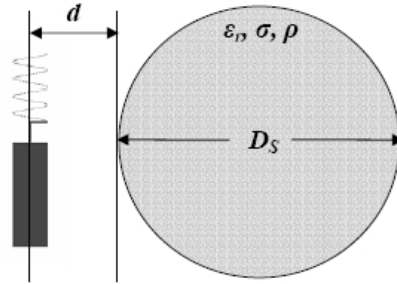


Figure 3. Helical handset-homogeneous sphere configuration.

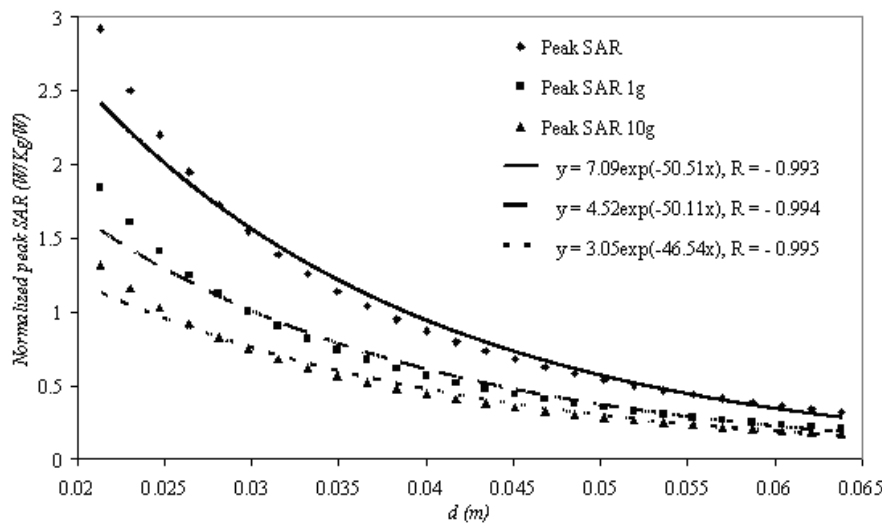


Figure 4. Variation of Peak SAR and Peak Average SAR over 1 g and 10 g for different distances d between axis of helix and outer surface of the homogeneous human head phantom.

is observed between the induced peak or average SAR values in the human phantom and the distance. A regression curve, based on correlation theory and applied to each series of results, certifies this allegation. The fitting criterion is the correlation coefficient R [17], with an absolute magnitude converging to unity. The exponential variation is absolutely prospective according to the studies presented in [13, 18, 19] and provides an additional verification of the enforced FDTD algorithm.

Table 2. Results of the driving point input impedance at each distance d between axis of helix and outer surface of the homogeneous human head phantom.

| $d(m)$ | $Z_{in}(\Omega)$ | $d(m)$ | $Z_{in}(\Omega)$ |
|--------|------------------|--------|------------------|
| 0.0213 | 48.35+8.88i | 0.0434 | 53.9+6.45i |
| 0.023 | 49.04+8.03i | 0.0451 | 54.21+6.4i |
| 0.0247 | 49.63+7.47i | 0.0468 | 54.5+6.35i |
| 0.0264 | 50.14+7.11i | 0.0485 | 54.78+6.27i |
| 0.0281 | 50.61+6.89i | 0.0502 | 55.05+6.19i |
| 0.0298 | 51.04+6.75i | 0.0519 | 55.3+6.1i |
| 0.0315 | 51.45+6.66i | 0.0536 | 55.54+6i |
| 0.0332 | 51.84+6.61i | 0.0553 | 55.77+5.89i |
| 0.0349 | 52.21+6.58i | 0.057 | 55.98+5.77i |
| 0.0366 | 52.57+6.56i | 0.0587 | 56.18+5.64i |
| 0.0383 | 52.92+6.54i | 0.0604 | 56.37+5.5i |
| 0.04 | 53.26+6.52i | 0.0621 | 56.53+5.36i |
| 0.0417 | 53.59+6.49i | 0.0638 | 56.69+5.21i |

In Table 2, the results of the calculated driving point input impedance Z_{in} of the helical handset antenna are presented for each position of the handset in front of the homogeneous human head phantom. The corresponding Standing Wave Ratio (SWR) for each case is then determined with respect to the free space input impedance as described in (3), (4):

$$SWR = \frac{1 + |\rho|}{1 - |\rho|} \quad (3)$$

$$\rho = \frac{Z_{in} - Z_{in}^{\text{free space}}}{Z_{in} + Z_{in}^{\text{free space}}} \quad (4)$$

where $Z_{in}^{\text{free space}} = 54.33 + j1.42\Omega$.

The induced peak and average SAR values at each position of the helical handset are apposed in Figure 5 as a function of the SWR at each respective configuration of the handset-sphere formation.

A regression curve is also applied to the simulation results to achieve adequate fitting. A logarithmic curve indicates a rather

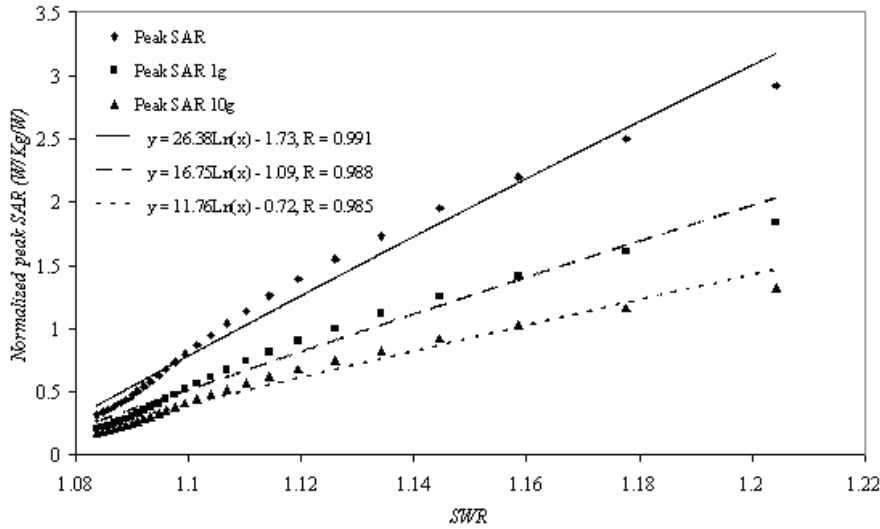


Figure 5. Variation of Peak SAR and Peak Average SAR over 1g and 10g with respect to SWR for each position between helix and homogeneous human head phantom.

approximate representation of the peak and average SAR values, providing a correlation coefficient converging to unity. Thus, for this specific configuration of the helical handset-human head model, a safe prediction of the induced peak and average SAR values can be attained regarding data from the mobile terminal e.g., SWR.

The concept of correlating the absorption mechanism of a biological tissue with the basic antenna parameters (e.g., input impedance, current, etc.) is not new. In [13], an analytic formula is given for the computation of the spatial peak SAR values induced in a plane phantom in the close near field of a radiating dipole. The study was based on the remark that the interaction between antenna and phantom is attributed to the surface currents produced by a plane wave incident magnetic field. The presented approximation formula provides a correlation of the peak SAR with the square of the incident magnetic field H_{tinc}^2 and consequently with the antenna current:

$$SAR = \frac{\sigma\mu\omega}{\rho\sqrt{\sigma^2 + \varepsilon^2\omega^2}} (1 + corr \cdot \gamma_{pw})^2 H_{tinc}^2 \quad (5)$$

where σ , μ , ε are the conductivity, the permeability and the permittivity of the biological tissue, ω is the radial frequency, H_{tinc} the magnetic field component of the incident plane wave and γ_{pw} the

plane wave reflection coefficient provided by the following equation:

$$\gamma_{pw} = \frac{2 \left| \sqrt{\varepsilon'} \right|}{\left| \sqrt{\varepsilon'} + \sqrt{\varepsilon_0} \right|} - 1 \quad (6)$$

where $\varepsilon' = \varepsilon - \frac{\sigma}{i\omega}$ is the complex permittivity and ε_0 the permittivity of free space. The correction factor *corr* accounts for the improper reflection properties at small distances d between antenna and tissue and is provided by the following equation:

$$corr = \begin{cases} 1, & \text{for } d \geq 0.08\lambda/\gamma_{pw} \\ \sin\left(\frac{\pi\gamma_{pw}d}{0.16\lambda}\right), & \text{for } d < 0.08\lambda/\gamma_{pw} \end{cases} \quad (7)$$

These formulas were derived by the application of the Generalized Multipole Technique (GMT). Simulation results revealed that the reflection coefficient $\gamma = \left(\frac{|H_{tsurf}|}{|H_{tinc}|} - 1\right)$, where H_{tsurf} stands for the spatial peak magnetic field at the surface of the phantom, approaches γ_{pw} and that the ratio of the magnitude of the electric field to the magnitude of the magnetic field ($|E|/|H|$) near the surface tissue approximates the wave impedance of the tissue. Moreover, (5) can be generalized to heterogeneous bodies of arbitrary shape and a maximum 3 dB variation is observed [13].

In the present study, the formula described in (5) is enforced to investigate its application to helical antennas. Thus, the term which has to be determined is the magnetic field component of the incident plane wave. To achieve this, the helix is assumed to stand alone (the handset box is eliminated), in order to be able to provide an expression of the incident magnetic field without the requirement of performing very complex electromagnetic analysis.

The helix antenna is assumed to consist of a series of dipoles and loops (specifically 4 loops, 3 dipoles and the helix final section above the handset), as in [7, 8] and consequently the equivalent magnetic component of the incident field is described by the H_φ and H_θ components for each radiator [1]:

$$|H_\varphi| = \frac{I \cdot L_d}{2 \cdot d \cdot \lambda} \quad (8)$$

$$|H_\theta| = \frac{\pi^2 \cdot I \cdot D_L}{4 \cdot d \cdot \lambda^2} \quad (9)$$

where I is the current of the helix antenna, L_d stands for the dipole length, d represents the distance from the helix axis, D_L is the

loop diameter and λ the wavelength at the frequency of propagation. Defining the diameter D_L as the helix radius and the dipole length L_d as the turns spacing, both drawn out from Table 1, the total incident magnetic field deriving from (8) and (9) is set in (5). The peak SAR induced in a biological tissue with the aforementioned dielectric characteristics of the homogeneous sphere is then computed at several distances and finally compared with the numerical results of the FDTD method. This comparison is demonstrated in Figure 6:

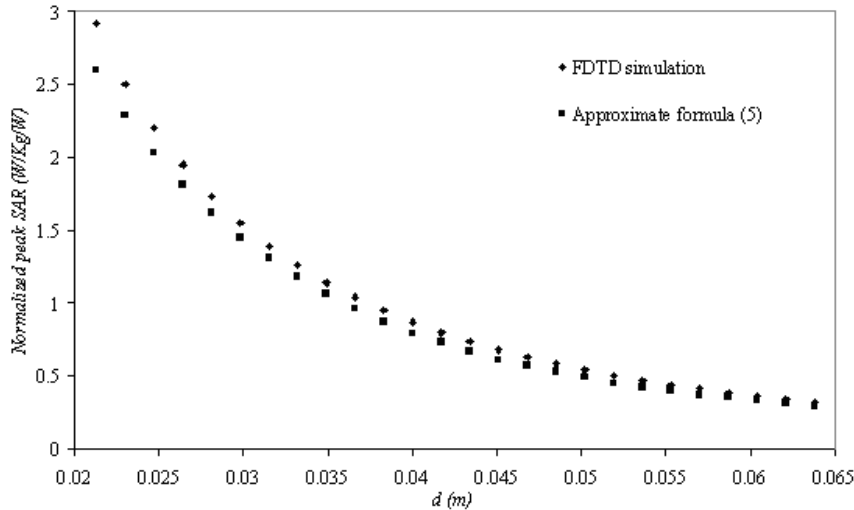


Figure 6. Comparison between the peak SAR values computed through FDTD and those derived from the approximation formula described in (5).

A rather satisfactory agreement is observed between the values calculated by the approximation formula of (5) and the FDTD numerical results. Consequently, the formula proposed by Kuster and Balzano [13] can be further applied to other handsets apart from the basic dipole antenna. Hence, a generalization of this specific formula for other antenna configurations is provided. It also reinforces the suggestion that the SAR induced in a biological tissue in the near field of a mobile handset antenna is strongly dependent on the current at the radiator. Thus, the variation of the SAR with regard to SWR depicted in Figure 5, implying a direct relation of the absorption mechanism to antenna parameters which can be practically evaluated (e.g., input impedance measurement), is additionally vindicated by the findings demonstrated in Figure 6.

4.2. Layered Phantom

To further investigate the absorption of a biological tissue illuminated by a helical handset, a spherical inhomogeneous human head model was utilized. This phantom consisted of three layers with materials simulating the human head structure, while the outer diameter was identical with that of the homogeneous sphere previously used. In Table 3, the type and the thickness of each layer and the corresponding relative permittivity, conductivity and density are depicted according to [26].

Table 3. Layer structure and values of relative permittivity, conductivity and density for each tissue.

| Layer (Type, thickness) | ϵ_r | σ | ρ |
|-------------------------|--------------|----------|--------|
| Skin, 6.8 mm | 41.41 | 0.867 | 1100 |
| Bone, 10.2 mm | 12.45 | 0.143 | 1200 |
| Brain, 85 mm | 45.81 | 0.767 | 1030 |

The FDTD scheme described in the previous section was also applied for this case and calculation of the peak and average SAR over 1 g and 10 g of tissue was conducted for several distances between the handset and the phantom. The results are graphically exhibited in Figure 7.

The exponential variation of the SAR values towards the separation between antenna and sphere is as well perceived in Figure 7 and verified by the applied regression curve. The input impedance of the helical handset was additionally assessed at each distance d and the results are presented in Table 4. Following the same procedure with the previous section, the alteration of the SAR with SWR at the helix is depicted in Figure 8, where again a logarithmic regression curve appears to best fit the simulation results ($R \cong 1$).

Finally, the formula presented in (5) was applied for the case of the inhomogeneous phantom and the resulting peak SAR values are shown in Figure 9 together with the corresponding to the same distance calculated values via the FDTD method.

The two sets of numerical results appear to be rather close, considering the uncertainty of 3 dB provided in [13]. Consequently, the generalization of this specific formula claimed in [13], is further verified for the use of helical handset antennas.

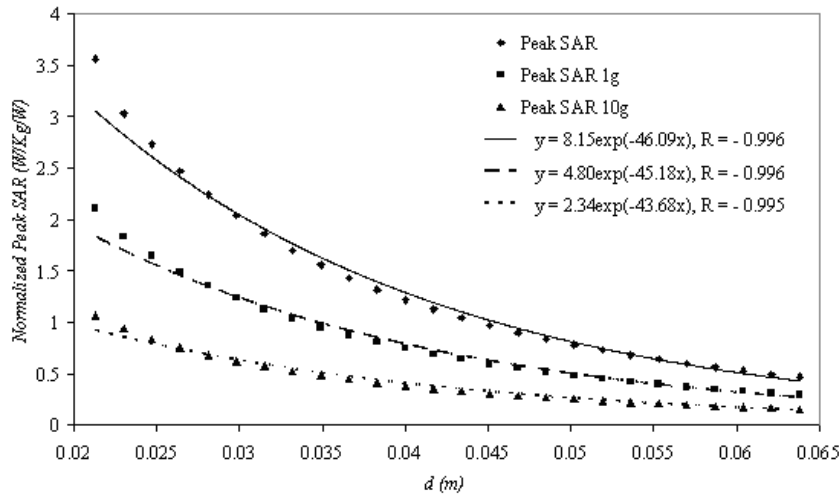


Figure 7. Variation of Peak SAR and Peak Average SAR over 1 g and 10 g for different distances d between axis of helix and outer surface of the heterogeneous human head phantom.

Table 4. Results of the driving point input impedance at each distance d between axis of helix and outer surface of the heterogeneous human head phantom.

| $d(m)$ | $Z_{in}(\Omega)$ | $d(m)$ | $Z_{in}(\Omega)$ |
|--------|------------------|--------|------------------|
| 0.0213 | 48.22+7.67i | 0.0434 | 53.27+6.05i |
| 0.023 | 48.84+6.87i | 0.0451 | 53.58+6.06i |
| 0.0247 | 49.35+6.36i | 0.0468 | 53.87+6.06i |
| 0.0264 | 49.81+6.06i | 0.0485 | 54.16+6.04i |
| 0.0281 | 50.22+5.89i | 0.0502 | 54.44+6.01i |
| 0.0298 | 50.6+5.81i | 0.0519 | 54.7+5.97i |
| 0.0315 | 50.96+5.79i | 0.0536 | 54.96+5.91i |
| 0.0332 | 51.31+5.81i | 0.0553 | 55.2+5.84i |
| 0.0349 | 51.66+5.85i | 0.057 | 55.43+5.76i |
| 0.0366 | 51.99+5.89i | 0.0587 | 55.65+5.67i |
| 0.0383 | 52.32+5.94i | 0.0604 | 55.86+5.57i |
| 0.04 | 52.64+5.99i | 0.0621 | 56.05+5.46i |
| 0.0417 | 52.96+6.02i | 0.0638 | 56.22+5.34i |

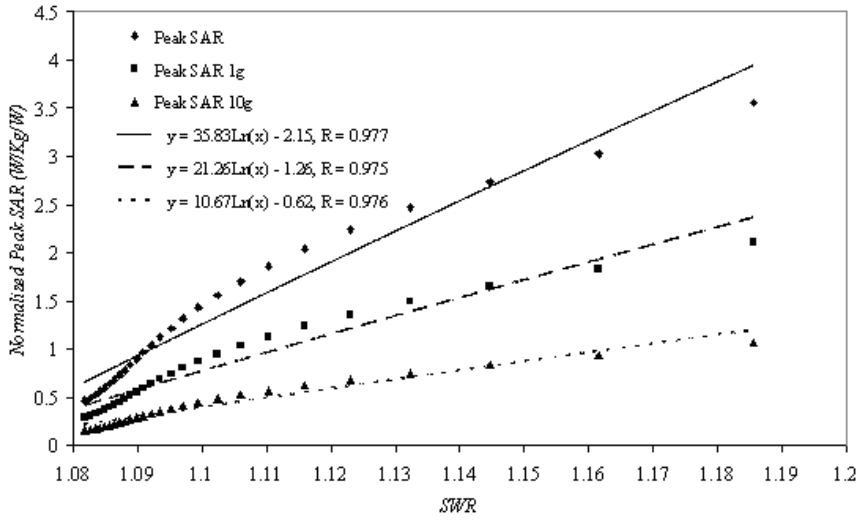


Figure 8. Variation of Peak SAR and Peak Average SAR over 1g and 10g with respect to SWR for each position between helix and heterogeneous human head phantom.

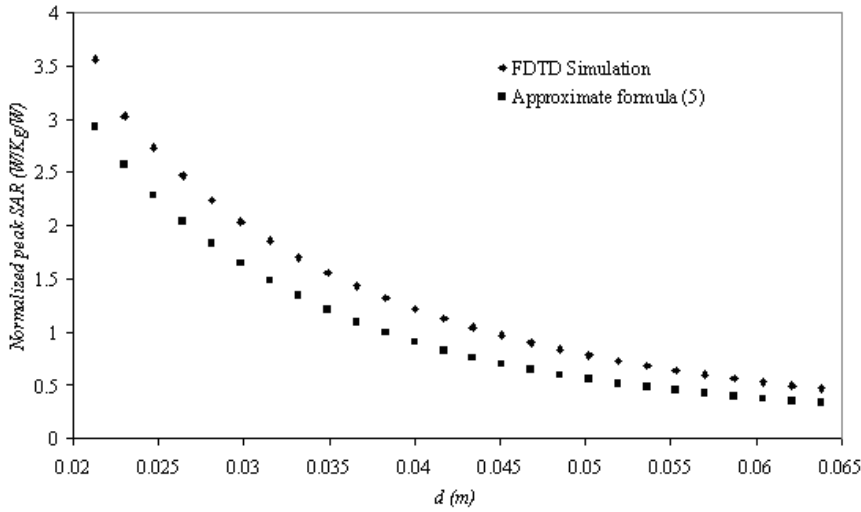


Figure 9. Comparison between the peak SAR values induced in the heterogeneous phantom computed through FDTD and those derived from the approximation formula described in (5).

5. CONCLUSIONS

A helical handset operating in front of a human head model was the subject of the present study. Following the optimization of the antenna structure, the FDTD method was applied to simulate the interaction of the mobile terminal with a spherical phantom. The results show that the energy absorbed by the biological tissue primary depends on the operational parameters of the handset's antenna and can be assessed through analytic formula or expressions derived from correlation and regression algorithms. The study extends the model provided by Kuster and Balzano so as to contain helical handsets, while additional results reveal the dependence of the SAR on the antenna characteristics (e.g., SWR). These can be easily measured and, thus, offer a real time estimation of the absorption level regarding the mobile terminal's position. Although the present investigation can not be directly applied to modern configurations of mobile handsets-human head models, the tendency to correlate the SAR with data derived from mobile antennas is indeed verified. In the future, the implementation of more realistic models of the human head (e.g., SAM phantoms) with precise structures of mobile terminals will provide an extension of the prediction procedures circumscribed in the current paper.

ACKNOWLEDGMENT

The work of Dr. N. K. Kouveliotes is supported by the EPEAEK-Pythagoras I research program. (The project is co-funded by the European Social Fund (75%) and National Resources (25%)).

REFERENCES

1. Kraus, J. D., *Antennas*, McGraw-Hill, New York, 1988.
2. Taflove, A., *Computational Electrodynamics: The Finite Difference Time Domain Method*, Artech House, Norwood, MA, 1995.
3. Poynting Software (Pty) Ltd., *SuperNecv. 2.4 MOM Technical Reference Manual*, [Online] Available <http://www.supernec.com/manuals/snmomtrm.htm>
4. Rowley, J. T., R. B. Waterhouse, and K. H. Joyner, "Modeling of normal-mode helical antennas at 900 MHz and 1.8 GHz for mobile communications handsets using the FDTD technique," *IEEE Trans. Antennas Propagat.*, Vol. 50, No. 6, 812–820, June 2002.
5. Hong, S.-W., M.-S. Park, H.-T. Oh, and C.-S. Park, "Arrayed

- helical antennas (AHA) with low SAR for personal telephone handsets," *Microwave Opt. Technol. Lett.*, Vol. 31, No. 4, 284–287, Nov. 2001.
6. Colburn, J. S. and Y. Rahmat-Samii, "Human proximity effects on circular polarized handset antennas in personal satellite communications," *IEEE Trans. Antennas Propagat.*, Vol. 46, No. 6, 813–820, June 1998.
 7. Lazzi, G. and O. P. Gandhi, "On modeling and personal dosimetry of cellular telephone helical antennas with the FDTD code," *IEEE Trans. Antennas Propagat.*, Vol. 46, No. 4, 525–530, April 1998.
 8. Lazzi, G., Q. S. Yu, and O. P. Gandhi, "Extension and validation of the equivalent sources helical antenna modeling with the FDTD code," *Proc. IEEE Antennas and Propagation Society Int. Symp.*, Vol. 2, 1054–1057, July 1999.
 9. Bernardi, P., M. Cavagnaro, S. Pisa, and E. Piuzzi, "Power absorption and temperature elevations induced in the human head by a dual-band monopole-helix antenna phone," *IEEE Trans. Microwave Theory Tech.*, Vol. 49, No. 12, 2539–2546, Dec. 2001.
 10. Bernardi, P., M. Cavagnaro, S. Pisa, and E. Piuzzi, "A graded-mesh FDTD code for the study of human exposure to cellular phones equipped with helical antennas," *Appl. Comput. Electromag. Soc. J.*, Vol. 16, 90–96, Mar. 2001.
 11. Dimbylow, P., M. Khalid, and S. Mann, "Assessment of specific energy absorption rate (SAR) in the head from a TETRA handset," *Phys. Med. Biol.*, Vol. 48, 3911–3926, 2003.
 12. Koulouridis, S. and K. S. Nikita, "Study of the coupling between human head and cellular phone helical antennas," *IEEE Trans. on Electromagn. Compat.*, Vol. 46, No. 1, 62–70, Feb. 2004.
 13. Kuster, N. and Q. Balzano, "Energy absorption mechanism by biological bodies in the near field of dipole antennas above 300 MHz," *IEEE Trans. on Veh. Technol.*, Vol. 41, No. 1, 17–23, Feb. 1992.
 14. King, R. W. P., "Electromagnetic field generated in model of human head by simplified telephone transceiver," *Radio Science*, Vol. 30, No. 1, 267–281, 1995.
 15. Riu, P. J., "Heating of tissue by near-field exposure to a dipole: A model analysis," *IEEE Trans. on Biomed. Engin.*, Vol. 46, No. 8, 911–917, 1999.
 16. Rahmat-Samii, Y. and E. Michielssen, *Electromagnetic Optimization by Genetic Algorithms*, John Wiley & Sons, Inc., 1999.
 17. McPherson, G., *Statistics in Scientific Investigation*, Springer-

- Verlag, New York, 1990.
18. Kouveliotes, N. K., P. J. Papakanellos, E. D. Nanou, N. I. Sakka, V. S. G. Tsiafakis, and C. N. Capsalis, "Correlation between SAR, SWR and distance of a mobile terminal antenna in front of a human phantom: Theoretical and experimental validation," *Journal of Electromagnetic Waves and Applications*, Vol. 17, No. 11, 1561–1581, 2003.
 19. Kouveliotes, N. K., P. T. Trakadas, and C. N. Capsalis, "Investigation of a dipole antenna performance and SAR distribution induced in a human head model," *Proc. 2nd International Workshop on Biological Effects of Electromagnetic Fields*, 813–819, 2002.
 20. Papakanellos, P. J., E. D. Nanou, N. I. Sakka, V. S. G. Tsiafakis, and C. N. Capsalis, "Near field interaction between a brain tissue equivalent phantom and a dipole antenna," *Proc. 2nd International Workshop on Biological Effects of Electromagnetic Fields*, 888–897, 2002.
 21. Fourie, A. and D. Nitch, "SuperNEC: antenna and indoor-propagation simulation program," *IEEE Antennas and Propagat. Mag.*, Vol. 42, No. 3, 31–48, June 2000.
 22. Ibrahim, A. and C. Dale, "Analysis of the temperature increase linked to the power induced by RF source," *Progress In Electromagnetics Research*, PIER 52, 23–46, 2005.
 23. Gao, S., "FDTD analysis of a dual-frequency microstrip patch antenna," *Progress In Electromagnetics Research*, PIER 54, 155–178, 2005.
 24. Eldek, A. A., A. Z. Elsherbeni, and C. E. Smith, "Dual-wideband square slot antenna with a U-shaped printed tuning stub for personal wireless communication systems," *Progress In Electromagnetics Research*, PIER 53, 319–333, 2005.
 25. Fang, J. and Z. Wu, "Generalized perfectly matched layer for the absorption of propagating and evanescent waves in lossless and lossy media," *IEEE Trans. Microwave Theory Tech.*, Vol. 44, No. 12, Dec. 1996.
 26. Federal Communications Commission, *Dielectric Properties of Body Tissues at RF and Microwave Frequencies*, [Online] Available <http://www.fcc.gov/fcc-bin/dielec.sh>